LETTER

doi:10.1038/nature22038

Therapeutic reduction of ataxin-2 extends lifespan and reduces pathology in TDP-43 mice

Lindsay A. Becker[1,2], Brenda Huang[1], Gregor Bieri[1,2], Rosanna Ma[1], David A. Knowles[1,3], Paymaan Jafar-Nejad[4], James Messing[5], Hong Joo Kim[5], Armand Soriano[4], Georg Auburger[6], Stefan M. Pulst[6], J. Paul Taylor[5,8], Frank Rigo[4] & Aaron D. Gitler[1]

Amyotrophic lateral sclerosis (ALS) is a rapidly progressing neurodegenerative disease that is characterized by motor neuron loss and that leads to paralysis and death 2–5 years after disease onset[1]. Nearly all patients with ALS have aggregates of the RNA-binding protein TDP-43 in their brains and spinal cords[2], and rare mutations in the gene encoding TDP-43 can cause ALS[3]. There are no effective TDP-43-directed therapies for ALS or related TDP-43 proteinopathies, such as frontotemporal dementia. Antisense oligonucleotides (ASOs) and RNA-interference approaches are emerging as attractive therapeutic strategies in neurological diseases[4]. Indeed, treatment of a rat model of inherited ALS (caused by a mutation in *Sod1*) with ASOs against *Sod1* has been shown to substantially slow disease progression[5]. However, as *SOD1* mutations account for only around 2–5% of ALS cases, additional therapeutic strategies are needed. Silencing TDP-43 itself is probably not appropriate, given its critical cellular functions[1,6]. Here we present a promising alternative therapeutic strategy for ALS that involves targeting ataxin-2. A decrease in ataxin-2 suppresses TDP-43 toxicity in yeast and flies[7], and intermediate-length polyglutamine expansions in the ataxin-2 gene increase risk of ALS[7,8]. We used two independent approaches to test whether decreasing ataxin-2 levels could mitigate disease in a mouse model of TDP-43 proteinopathy[9]. First, we crossed ataxin-2 knockout mice with *TDP-43* (also known as *TARDBP*) transgenic mice. The decrease in ataxin-2 reduced aggregation of TDP-43, markedly increased survival and improved motor function. Second, in a more therapeutically applicable approach, we administered ASOs targeting ataxin-2 to the central nervous system of *TDP-43* transgenic mice. This single treatment markedly extended survival. Because TDP-43 aggregation is a component of nearly all cases of ALS[6], targeting ataxin-2 could represent a broadly effective therapeutic strategy.

To test the hypothesis that a decrease in ataxin-2 levels can rescue neurodegenerative phenotypes caused by TDP-43 accumulation, we first used a genetic approach. There are several transgenic mouse lines that express wild-type or mutant TDP-43, using various strategies[10]. We selected a mouse line that expressed human wild-type TDP-43 under the control of the Thy1 promoter, which drives pan-neuronal expression starting at around postnatal day seven (P7). We chose this mouse line because it presents robust and consistent phenotypes caused by abnormal TDP-43 accumulation. Whereas mice hemizygous for the *TDP-43* transgene (*TDP-43*$^{Tg/+}$) are viable, fertile, and grossly normal, mice that have two copies of this transgene (*TDP-43*$^{Tg/Tg}$) display profound motor dysfunction, resulting in an inability to walk around P21 and death around P24 (refs 9, 11). In this study, we euthanized the animals when they were no longer able to right themselves after falling on their side. This humane euthanasia endpoint is a distinct advantage of this TDP-43 mouse model, because it is directly dependent on motor dysfunction, an ALS-relevant phenotype. The degenerating neurons in the brain and spinal cord of *TDP-43*$^{Tg/Tg}$ mice contain ubiquitinated and phosphorylated TDP-43 aggregates, the pathological hallmark of ALS patients[2]. This rapidly progressing phenotype provided a powerful readout of disease suppression to test potential therapeutic interventions. To decrease ataxin-2 we used two independently generated lines of ataxin-2 knockout mice on different genetic backgrounds (see Methods). Heterozygous (*Atxn2*$^{+/-}$) and homozygous (*Atxn2*$^{-/-}$) mice are viable and fertile, with *Atxn2*$^{-/-}$ mice exhibiting some mid-life-onset obesity phenotypes[12,13]. We crossed *TDP-43*$^{Tg/+}$ mice with *Atxn2*$^{+/-}$ mice to produce *TDP-43*$^{Tg/+}$*Atxn2*$^{+/-}$ offspring and then intercrossed these mice to produce *TDP-43*$^{Tg/Tg}$*Atxn2*$^{+/+}$, *TDP-43*$^{Tg/Tg}$*Atxn2*$^{+/-}$, *TDP-43*$^{Tg/Tg}$*Atxn2*$^{-/-}$ and wild-type littermates (see Methods).

Decreased levels of ataxin-2 in *TDP-43*$^{Tg/Tg}$*Atxn2*$^{+/-}$ mice significantly improved lifespan compared to *TDP-43*$^{Tg/Tg}$*Atxn2*$^{+/+}$ (Fig. 1a) and complete removal of ataxin-2 in *TDP-43*$^{Tg/Tg}$*Atxn2*$^{-/-}$ mice resulted in a pronounced 80% improvement in median lifespan (Fig. 1b), with several *TDP-43*$^{Tg/Tg}$*Atxn2*$^{-/-}$ mice surviving more than 400 days. None of the *TDP-43*$^{Tg/Tg}$*Atxn2*$^{+/+}$ mice survived more than 29 days. We observed significant lifespan extension upon ataxin-2 reduction in both mouse lines we created (Extended Data Fig. 1 a–d). Within the entire *TDP-43*$^{Tg/Tg}$*Atxn2*$^{-/-}$ population, we found evidence for two groups of responders (strong and weak), and the genetic background of the mice significantly contributed to this variability (Cox proportional hazards $P = 0.002$, line A:B hazard ratio (HR) = 6.8; Extended Data Fig. 1f).

In addition to extending survival, decreased ataxin-2 slowed disease progression and improved motor function. All mice were able to walk efficiently by P13 (Supplementary Videos 1, 2). As previously described[9], *TDP-43*$^{Tg/Tg}$ mice started to display a mild tremor and had some difficulty walking around P15, which steadily progressed to a severe tremor and complete lack of joint movement in the hindlimbs around P21 (Supplementary Video 3). Reducing ataxin-2 levels in *TDP-43*$^{Tg/Tg}$*Atxn2*$^{+/-}$ and *TDP-43*$^{Tg/Tg}$*Atxn2*$^{-/-}$ animals significantly decreased gait impairment scores (see Methods) starting at P15 (Fig. 1c) and slowed the rate of progression of the gait impairment (Fig. 1d). Decreased ataxin-2 also mitigated tremor (Fig. 1e) and kyphosis (hunched posture that can be caused by neurodegeneration; Fig. 1f). Even after an age at which all *TDP-43*$^{Tg/Tg}$*Atxn2*$^{+/+}$ mice had reached the humane euthanasia endpoint (Supplementary Video 4), several of the *TDP-43*$^{Tg/Tg}$*Atxn2*$^{-/-}$ mice had no overt motor dysfunction (Supplementary Video 5). We confirmed that *TDP-43*$^{Tg/Tg}$*Atxn2*$^{+/+}$ mice had an approximately 30% decrease in cortical layer V pyramidal neurons and an approximately 27% decrease in lower motor neurons[9]. We found a significant rescue of layer V neurons and a trend towards lower motor neuron rescue in *TDP-43*$^{Tg/Tg}$*Atxn2*$^{-/-}$ mice (Extended Data Fig. 2).

Reducing the levels of ataxin-2 did not affect mRNA or protein levels of the human TDP-43 transgene in mouse brain tissue (Extended

[1]Department of Genetics, Stanford University School of Medicine, Stanford, California 94305, USA. [2]Stanford Neurosciences Graduate Program, Stanford University School of Medicine, Stanford, California 94305, USA. [3]Department of Radiology, Stanford University School of Medicine, Stanford, California 94305, USA. [4]Ionis Pharmaceuticals, Carlsbad, California 92010, USA. [5]Department of Cell and Molecular Biology, St. Jude Children's Research Hospital, Memphis, Tennessee 38105, USA. [6]Experimental Neurology, Department of Neurology, Goethe University, 60590 Frankfurt am Main, Germany. [7]Department of Neurology, University of Utah, Salt Lake City, Utah 84112, USA. [8]Howard Hughes Medical Institute, Chevy Chase, Maryland 20815, USA.

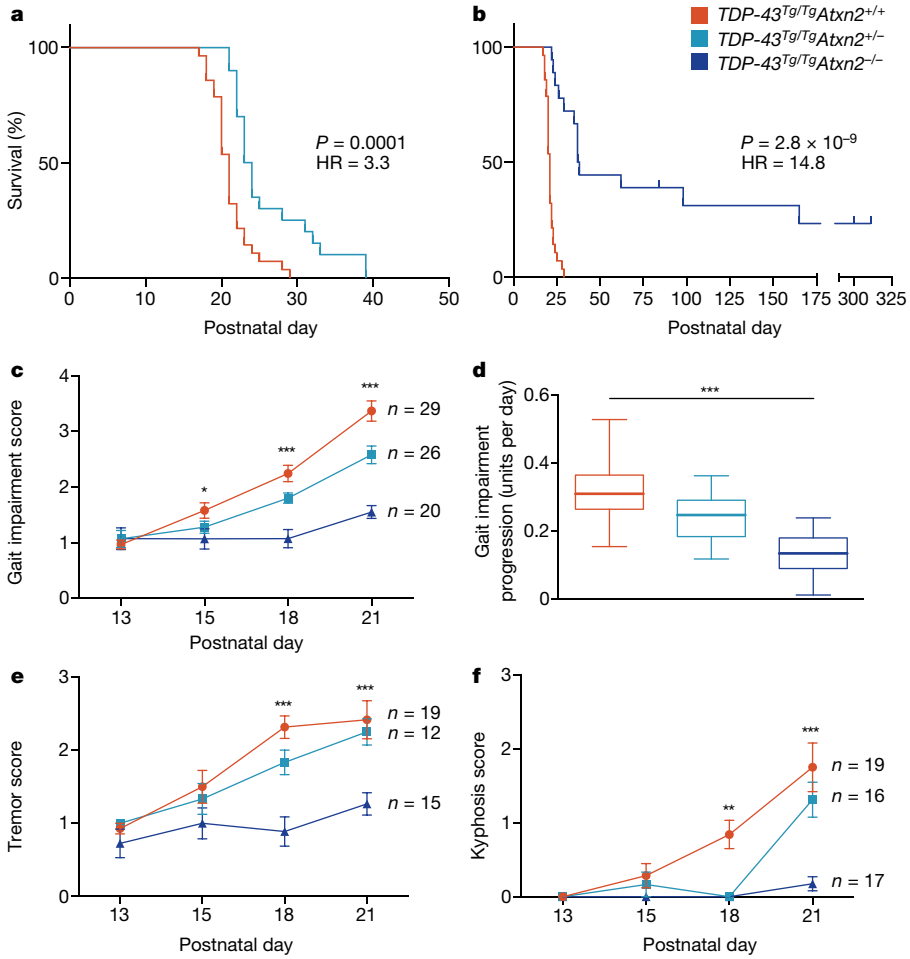

Figure 1 | A reduction in the level of ataxin-2 extends lifespan, improves motor function, and slows the rate of disease progression in TDP-43 transgenic mice. a, **b**, Kaplan–Meier survival curves comparing the survival of *TDP-43*$^{Tg/Tg}$*Atxn2*$^{+/+}$ ($n = 28$), *TDP-43*$^{Tg/Tg}$*Atxn2*$^{+/-}$ ($n = 20$) and *TDP-43*$^{Tg/Tg}$*Atxn2*$^{-/-}$ ($n = 18$) mice. Curves were compared by log-rank test, and effect size was estimated by a Cox proportional hazards model. HR, hazard ratio. Ticks indicate mice that were euthanized for tissue collection before reaching the humane euthanasia endpoint or that were still alive at the time of submission of this manuscript (see Methods). **c**, The gait impairment score of *TDP-43*$^{Tg/Tg}$ mice became worse with age, but this was attenuated by decreased levels of ataxin-2. **d**, A line was fit to the gait scores of each mouse over time and the slope of that line was plotted, grouping animals by genotype. The error bars are minimum to maximum, and the three groups were compared by a one-way ANOVA. **e**, **f**, Tremor and kyphosis scores were also decreased by a reduction in ataxin-2 in *TDP-43*$^{Tg/Tg}$ mice. **c**, **e**, **f**, At each age, the three genotypes were compared by one-way ANOVA. Combined data from lines A and B are shown. Data are mean ± s.e.m. $*P < 0.05$, $**P < 0.01$, $***P < 0.001$.

Data Figs 3, 4). Total TDP-43 (human and mouse) protein levels were also not significantly affected by ataxin-2 reduction (Extended Data Fig. 4). Therefore, the beneficial effect of decreased ataxin-2 levels does not appear to act by reducing TDP-43 expression.

Ataxin-2 is an RNA-binding protein with multiple roles in RNA metabolism, including regulation of stress granule assembly[14,15]. Stress granules are highly dynamic, transient intracellular accumulations of RNA and protein that form when translation is stalled in response to cellular stress. We and others have proposed that the concentration of aggregation-prone proteins like TDP-43 in stress granules can lead to the formation of pathological protein aggregates in ALS[16,17]. Stress granule formation increases the levels of insoluble TDP-43, and TDP-43 inclusions can persist after stress granule dissolution[18,19]. Several lines of evidence suggest that TDP-43 inclusion formation may be involved directly in disease progression. ALS-associated mutations in TDP-43 increase the aggregation propensity and/or stability of the protein[6,19,20]. Additionally, TDP-43 inclusion pathology is correlated with neuron death in ALS patients[21] and disease severity in TDP-43 mouse models[9–11]. Therefore, we hypothesized that decreasing ataxin-2 might reduce the propensity of TDP-43 to transit to stress granules and subsequently form pathological aggregates, and that this could prevent neurodegeneration.

To investigate the mechanism by which ataxin-2 levels influence TDP-43, we first performed experiments with cultured human cells to visualize stress granule dynamics. Stress granules formed rapidly and, over time, underwent a maturation process in which they fused to form larger structures (Fig. 2a), consistent with their liquid-like material properties[22]. We knocked down ataxin-2 with short interfering RNA (siRNA) and this markedly delayed the maturation of stress granules—at each time point, the stress granules were smaller and more numerous than in the cells treated with control siRNA (Fig. 2a–c). Endogenous TDP-43 was recruited to stress granules, consistent with previous reports[19], and was readily recognized by phosphorylation-specific and C-terminal epitope TDP-43 antibodies (Extended Data Fig. 5). Knocking down ataxin-2 significantly decreased the proportion of cells with stress granules containing endogenous TDP-43 (Fig. 2e, f). These data provide evidence that a reduction in ataxin-2 leads to modulated stress granule dynamics and decreased recruitment of TDP-43 to stress granules. We hypothesize that inhibition of the recruitment of TDP-43 into stress granules might reduce the propensity of TDP-43 to form pathological inclusions.

We next tested our hypothesis *in vivo* by determining the effect of decreased ataxin-2 levels on TDP-43 inclusion formation in *TDP-43* transgenic mice. Aggregated TDP-43 in neurons of ALS patients can

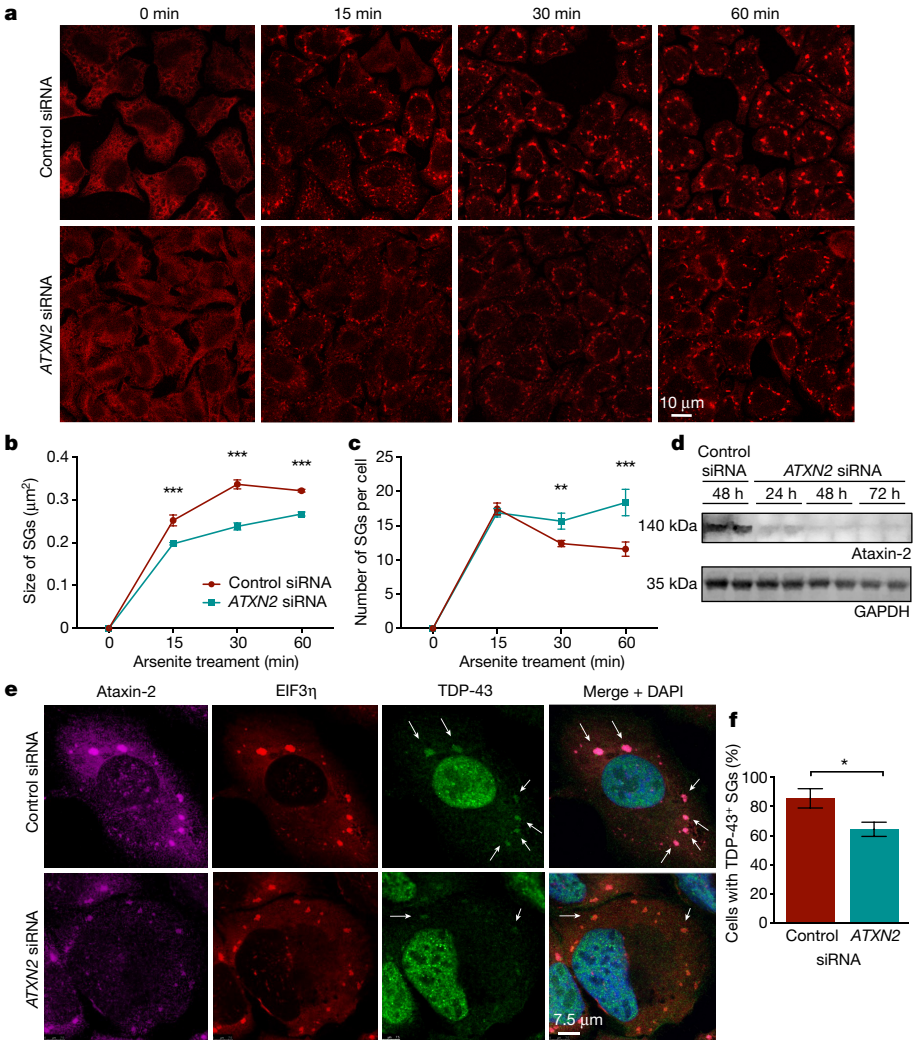

Figure 2 | Knockdown of ataxin-2 delays the maturation of stress granules and decreases recruitment of TDP-43 to stress granules. a, An EIF3η antibody was used to visualize stress granules (SGs) in U2OS cells. During continued stress, stress granules fuse to form larger structures. *ATXN2* siRNA inhibited maturation of stress granules, resulting in smaller, more numerous stress granules at each time point. **b**, **c**, Quantification of size (**b**) and number (**c**) of stress granules. **d**, Western blot of ataxin-2 knockdown. Gel source data can be found in Supplementary Fig. 1. **e**, **f**, Ataxin-2 siRNA treatment caused fewer cells to have TDP-43-positive stress granules at 60 min of arsenite exposure. **b**, **c**, **f**, The mean ± s.e.m. of three separate wells (116–146 cells per well) is plotted for each data point. Two-tailed *t*-tests were used to compare treatment groups. $*P < 0.05$, $**P < 0.01$, $***P < 0.001$.

become detergent insoluble, phosphorylated and cleaved to form C-terminal fragments (CTFs). It is not clear what role these alterations play in pathogenesis, but they are highly correlated with, and indicative of, pathological inclusion formation[23,24]. We found that RIPA-insoluble, urea-soluble full-length TDP-43 was four times higher in *TDP-43*$^{Tg/Tg}$*Atxn2*$^{+/+}$ mice than wild-type littermates (Fig. 3a, b). We also detected insoluble TDP-43 CTFs in TDP-43 transgenic mice (Fig. 3a, c). Reduced ataxin-2 moderately decreased levels of insoluble full-length and CTF TDP-43 (Fig. 3a–c). To visualize TDP-43 inclusions, we performed immunohistochemistry on spinal cord sections of TDP-43 transgenic mice. We used three different phosphorylation (p)-specific TDP-43 antibodies (pTDP-43 antibodies 1–3 (ab1–ab3)). We detected round, predominantly nuclear inclusions in *TDP-43*$^{Tg/Tg}$ mice when immunostaining with pTDP-43 ab1 or with TDP-43 antibodies that are not phosphorylation-specific (Extended Data Fig. 6e, f, q, s). The other two pTDP-43 antibodies tested (pTDP-43 ab2 and ab3) recognized nuclear and cytoplasmic inclusions that were much more numerous (Extended Data Fig. 6g). We did not detect inclusions in wild-type littermates with any of the TDP-43 antibodies tested (Extended Data Fig. 6a–d, m–p). Additionally, we found that cells with nuclear inclusions had lower levels of diffuse nuclear TDP-43 staining (Extended Data Fig. 6u). This suggests that inclusion formation may sequester TDP-43 and cause a partial loss of TDP-43 function, which can be toxic to neurons *in vivo*[25]. To investigate whether ataxin-2 reduction had an effect on TDP-43 pathology, we quantified spinal cord inclusions and found that pTDP-43 ab1-positive and pTDP-43 ab2-positive inclusions were reduced by 75% and 45%, respectively, in *TDP-43*$^{Tg/Tg}$*Atxn2*$^{-/-}$ mice (Fig. 3d–h). These results support the hypothesis that reduced ataxin-2 mitigates TDP-43 toxicity by decreasing the propensity of TDP-43 to form pathological aggregates.

Given the notable amelioration of disease seen with ataxin-2 genetic reduction, we sought to further explore the translational potential of decreasing ataxin-2 levels in a more therapeutically applicable manner using ASOs. ASOs are highly stable, synthetic nucleic acids that specifically hybridize with an mRNA target, triggering RNase-H-mediated cleavage and degradation of the mRNA while leaving the ASO intact[4]. We screened a collection of ASOs for safety and efficacy (Extended Data Fig. 7 and see Scoles *et al.*[26]), and used the most effective and well-tolerated ASO for further studies. Intracerebroventricular (ICV) injection of the *Atxn2*-targeting ASO at P1 did not affect the home-cage behaviour or grip strength of wild-type mice (Extended Data Fig. 7d). We also did not detect an increase in

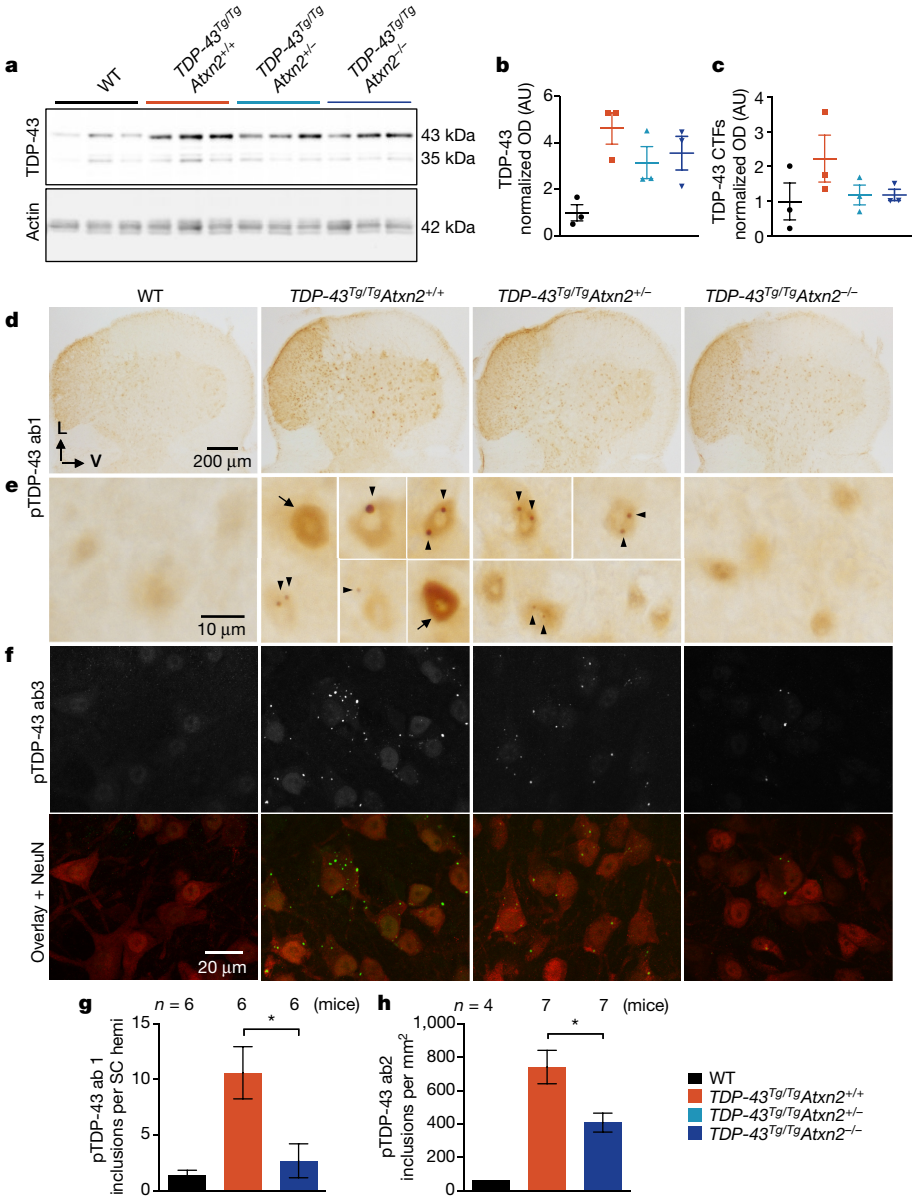

Figure 3 | Reduced ataxin-2 levels decrease TDP-43 pathology. a–c, RIPA-insoluble, urea-soluble full-length (43 kDa) and CTF TDP-43 (35 kDa) are increased in *TDP-43*$^{Tg/Tg}$ *Atxn2*$^{+/+}$ mice (quantified in **b**, **c**), and appeared moderately reduced in *TDP-43*$^{Tg/Tg}$ *Atxn2*$^{-/-}$ mice. Gel source data can be found in Supplementary Fig. 1. **d**, Lumbar spinal cord hemispheres (SC hemi) stained with pTDP-43 ab1. **e**, Magnification to the cellular level reveals weak, diffuse nuclear staining in wild-type mice, and pTDP-43 inclusions (arrow heads) and strong diffuse nuclear pTDP-43 (arrows) in *TDP-43*$^{Tg/Tg}$*Atxn2*$^{+/+}$ mice. Fluorescent stains (Extended Data Fig. 6e) demonstrate that most pTDP-43 ab1 inclusions are nuclear. **f**, Staining with pTDP-43 ab3 reveals inclusions that are much more numerous and usually cytoplasmic (Extended Data Fig. 6g). **g**, **h**, A reduction in ataxin-2 decreased pTDP-43 ab1 inclusions at P21 (**g**), and pTDP-43 ab2 inclusions at P23 (**h**) in the lumbar spinal cord. Two-tailed *t*-tests were performed between groups of interest. Data are mean ± s.e.m. $^*P < 0.05$.

expression of genes associated with astroglial and microglial activation or inflammation (Extended Data Fig. 7e–i), suggesting that this dose of ASO did not produce adverse side effects.

To test whether *Atxn2*-targeting ASOs could mitigate disease in *TDP-43* transgenic mice, we treated *TDP-43* transgenic mice and wild-type littermates with a one-time ICV injection of a non-targeting control ASO or *Atxn2* ASO at P1 (Fig. 4a). Both ASOs were well tolerated by the mice at this dose, and the *Atxn2* ASO successfully reduced levels of *Atxn2* mRNA by 77% on average when assessed at P21 (Fig. 4b). Neither ASO affected expression levels of the human *TDP-43* transgene (Fig. 4c). *TDP-43* transgenic mice injected with the *Atxn2* ASO had a notable 35% increase in median lifespan compared to littermates injected with the control ASO (Fig. 4d) and had significantly improved motor performance by P21 (Fig. 4e; Supplementary Video 6). Two of the sixteen *TDP-43*$^{Tg/Tg}$ mice treated with *Atxn2* ASO survived over 120 days, whereas no *TDP-43*$^{Tg/Tg}$ mouse treated with the control ASO lived past 32 days. Therefore, a single administration of *Atxn2*-targeting ASOs into the central nervous system is sufficient to greatly prolong survival and improve motor performance of *TDP-43* transgenic mice.

We have shown by two independent approaches that a decrease of ataxin-2 levels markedly increases lifespan and improves motor function in *TDP-43* transgenic mice. Additionally, we have demonstrated that reduced ataxin-2 decreases the burden of TDP-43 inclusions, which provides mechanistic evidence that ataxin-2 may modulate toxicity by affecting the aggregation propensity of TDP-43. In support of this hypothesis, ataxin-2 and TDP-43 physically interact in an RNA-dependent manner, and ALS-associated polyglutamine expansions in ataxin-2, which enhance stability[7], can increase TDP-43 pathological modifications[27]. We demonstrate that decreased ataxin-2 impairs the maturation of stress granules, which are hypothesized to facilitate the pathological aggregation of TDP-43 (refs 16, 17). Indeed, a reduction in ataxin-2 in cultured cells decreases recruitment of endogenous TDP-43 to stress granules. Beyond ataxin-2, this general strategy of targeting factors required for the assembly of ribonucleoprotein granules could be pursued as a way to mitigate TDP-43 pathological aggregation and neurodegeneration.

Reduction of ataxin-2 has exciting therapeutic potential for ALS and frontotemporal dementia, because TDP-43 pathology is a component of 97% of ALS cases and nearly 50% of frontotemporal dementia cases[6]. Although complete knockout of ataxin-2 seems well tolerated in mouse, further preclinical studies are required to assess the long-term safety and efficacy of ataxin-2 knockdown in the mammalian central nervous system. It is, perhaps, inspiring that there are currently clinical trials to test ASO therapies for Huntington's disease (targeting *HTT*)[28], familial

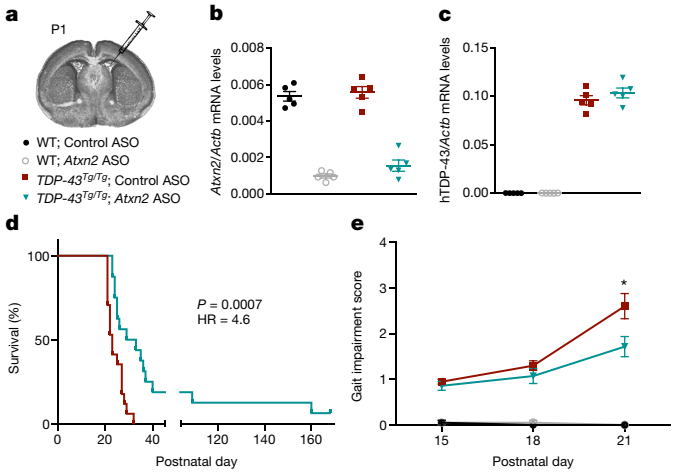

Figure 4 | ASOs that target ataxin-2 extend lifespan and improve motor performance in TDP-43 transgenic mice. a, P1 mouse pups were treated with control or *Atxn2* ASOs by ICV injection. **b**, **c**, At P21, mRNA levels of *Atxn2* were decreased by 77% in the brains of mice injected with the *Atxn2* ASO (**b**) without affecting mRNA levels of the human *TDP-43* transgene (**c**). **d**, Lifespan was significantly extended by treatment with the *Atxn2* ASO ($n = 16$) compared to the control ASO ($n = 17$). Curves were compared by log-rank test, and effect size was estimated using a Cox proportional hazards model. The tick indicates a mouse still alive at the time of submission. **e**, Gait impairment score was also improved in mice treated with the *Atxn2* ASO ($n = 14$) by P21 compared to treatment with the control ASO ($n = 20$). Two-tailed *t*-tests were used to compare the two treatment groups at each age. Data are mean ± s.e.m. $^*P < 0.05$.

ALS (targeting *SOD1*)[29], and spinal muscular atrophy (targeting *SMN2* splicing)[30]. Indeed, in patients with familial ALS caused by *SOD1* mutations, ASOs targeting *SOD1* administered as an intrathecal infusion were well tolerated[29]. Reducing ataxin-2 levels to treat TDP-43 proteinopathy is the first proposed ASO therapy for neurodegenerative disease designed to target a modifier gene that is not directly causative of the disease. This type of approach will probably be essential for treating sporadic ALS, which makes up over 90% of cases, because of the vital cellular role of TDP-43.

Online Content Methods, along with any additional Extended Data display items and Source Data, are available in the online version of the paper; references unique to these sections appear only in the online paper.

Received 3 June 2016; accepted 2 March 2017.
Published online 12 April 2017.

1. Taylor, J. P., Brown, R. H., Jr & Cleveland, D. W. Decoding ALS: from genes to mechanism. *Nature* **539,** 197–206 (2016).
2. Neumann, M. *et al.* Ubiquitinated TDP-43 in frontotemporal lobar degeneration and amyotrophic lateral sclerosis. *Science* **314,** 130–133 (2006).
3. Lagier-Tourenne, C. & Cleveland, D. W. Rethinking ALS: the FUS about TDP-43. *Cell* **136,** 1001–1004 (2009).
4. Southwell, A. L., Skotte, N. H., Bennett, C. F. & Hayden, M. R. Antisense oligonucleotide therapeutics for inherited neurodegenerative diseases. *Trends Mol. Med.* **18,** 634–643 (2012).
5. Smith, R. A. *et al.* Antisense oligonucleotide therapy for neurodegenerative disease. *J. Clin. Invest.* **116,** 2290–2296 (2006).
6. Ling, S. C., Polymenidou, M. & Cleveland, D. W. Converging mechanisms in ALS and FTD: disrupted RNA and protein homeostasis. *Neuron* **79,** 416–438 (2013).
7. Elden, A. C. *et al.* Ataxin-2 intermediate-length polyglutamine expansions are associated with increased risk for ALS. *Nature* **466,** 1069–1075 (2010).
8. Sproviero, W. *et al. ATXN2* trinucleotide repeat length correlates with risk of ALS. *Neurobiol. Aging* **51,** 178.e1–178.e9 (2017).
9. Wils, H. *et al.* TDP-43 transgenic mice develop spastic paralysis and neuronal inclusions characteristic of ALS and frontotemporal lobar degeneration. *Proc. Natl Acad. Sci. USA* **107,** 3858–3863 (2010).
10. McGoldrick, P., Joyce, P. I., Fisher, E. M. & Greensmith, L. Rodent models of amyotrophic lateral sclerosis. *Biochim. Biophys. Acta* **1832,** 1421–1436 (2013).
11. Janssens, J. *et al.* Overexpression of ALS-associated p.M337V human TDP-43 in mice worsens disease features compared to wild-type human TDP-43 mice. *Mol. Neurobiol.* **48,** 22–35 (2013).
12. Kiehl, T. R. *et al.* Generation and characterization of Sca2 (ataxin-2) knockout mice. *Biochem. Biophys. Res. Commun.* **339,** 17–24 (2006).
13. Lastres-Becker, I. *et al.* Insulin receptor and lipid metabolism pathology in ataxin-2 knock-out mice. *Hum. Mol. Genet.* **17,** 1465–1481 (2008).
14. Nonhoff, U. *et al.* Ataxin-2 interacts with the DEAD/H-box RNA helicase DDX6 and interferes with P-bodies and stress granules. *Mol. Biol. Cell* **18,** 1385–1396 (2007).
15. Kaehler, C. *et al.* Ataxin-2-like is a regulator of stress granules and processing bodies. *PLoS One* **7,** e50134 (2012).
16. Ramaswami, M., Taylor, J. P. & Parker, R. Altered ribostasis: RNA–protein granules in degenerative disorders. *Cell* **154,** 727–736 (2013).
17. Li, Y. R., King, O. D., Shorter, J. & Gitler, A. D. Stress granules as crucibles of ALS pathogenesis. *J. Cell Biol.* **201,** 361–372 (2013).
18. Parker, S. J. *et al.* Endogenous TDP-43 localized to stress granules can subsequently form protein aggregates. *Neurochem. Int.* **60,** 415–424 (2012).
19. Liu-Yesucevitz, L. *et al.* Tar DNA binding protein-43 (TDP-43) associates with stress granules: analysis of cultured cells and pathological brain tissue. *PLoS One* **5,** e13250 (2010).
20. Johnson, B. S. *et al.* TDP-43 is intrinsically aggregation-prone, and amyotrophic lateral sclerosis-linked mutations accelerate aggregation and increase toxicity. *J. Biol. Chem.* **284,** 20329–20339 (2009).
21. Geser, F. *et al.* Evidence of multisystem disorder in whole-brain map of pathological TDP-43 in amyotrophic lateral sclerosis. *Arch. Neurol.* **65,** 636–641 (2008).
22. Molliex, A. *et al.* Phase separation by low complexity domains promotes stress granule assembly and drives pathological fibrillization. *Cell* **163,** 123–133 (2015).
23. Neumann, M. *et al.* Phosphorylation of S409/410 of TDP-43 is a consistent feature in all sporadic and familial forms of TDP-43 proteinopathies. *Acta Neuropathol.* **117,** 137–149 (2009).
24. Igaz, L. M. *et al.* Expression of TDP-43 C-terminal fragments *in vitro* recapitulates pathological features of TDP-43 proteinopathies. *J. Biol. Chem.* **284,** 8516–8524 (2009).
25. Yang, C. *et al.* Partial loss of TDP-43 function causes phenotypes of amyotrophic lateral sclerosis. *Proc. Natl Acad. Sci. USA* **111,** E1121–E1129 (2014).
26. Scoles, D. R. *et al.* Antisense oligonucleotide therapy for spinocerebellar ataxia type 2. *Nature* http://dx.doi.org/10.1038/nature22044 (2017).
27. Hart, M. P. & Gitler, A. D. ALS-associated ataxin 2 polyQ expansions enhance stress-induced caspase 3 activation and increase TDP-43 pathological modifications. *J. Neurosci.* **32,** 9133–9142 (2012).
28. Kordasiewicz, H. B. *et al.* Sustained therapeutic reversal of Huntington's disease by transient repression of huntingtin synthesis. *Neuron* **74,** 1031–1044 (2012).
29. Miller, T. M. *et al.* An antisense oligonucleotide against SOD1 delivered intrathecally for patients with SOD1 familial amyotrophic lateral sclerosis: a phase 1, randomised, first-in-man study. *Lancet Neurol.* **12,** 435–442 (2013).
30. Finkel, R. S. *et al.* Treatment of infantile-onset spinal muscular atrophy with nusinersen: a phase 2, open-label, dose-escalation study. *Lancet* **388,** 3017–3026 (2016).

Supplementary Information is available in the online version of the paper.

Acknowledgements This work was supported by NIH grants R01NS065317, R01NS09386501, R01NS073660 and R35NS097263 (10) (A.D.G.), NIH grant R35NS097974 (J.P.T), HHMI (J.P.T), NIH grants R21NS081182 and R37NS033123 (S.M.P), the National Science Foundation Graduate Research Fellowship (L.A.B.), the Robert Packard Center for ALS Research at Johns Hopkins (A.D.G.), Target ALS (A.D.G.), the Glenn Foundation (A.D.G.), and the DFG grant AU96/13-1 (G.A.). We thank L. Petrucelli and V. Lee for sharing TDP-43 antibodies, J. Shorter and L. Petrucelli for comments on the manuscript and discussions, A. Olsen and the Stanford Neuroscience Microscopy Service, supported by a grant from NIH (NS069375), for help with the confocal images, Y. Zuber (Stanford Veterinary Service Center) for mouse husbandry advice and support, Stanford's Human Immune Monitoring Center (HIMC) for performing the Luminex assays.

Author Contributions L.A.B. and A.D.G. designed the experiments and wrote the paper. All authors reviewed and edited the manuscript. L.A.B. performed experiments and analysed data. B.H. performed ASO injections and behavioural analyses on ASO-treated animals. G.B. helped with mouse dissections, and R.M. helped with mouse breeding and husbandry. D.A.K. helped perform statistical analyses. P.J.-N., A.S. and F.R. contributed ASOs, performed experiments to test ataxin-2 knockdown and immune response, and provided advice on designing experiments. J.M. and H.J.K. performed *in vitro* stress granule experiments. J.P.T. helped analyse stress granule experiments. G.A. and S.M.P. provided ataxin-2 knockout mice.

Author Information Reprints and permissions information is available at www.nature.com/reprints. The authors declare competing financial interests: details are available in the online version of the paper. Readers are welcome to comment on the online version of the paper. Publisher's note: Springer Nature remains neutral with regard to jurisdictional claims in published maps and institutional affiliations. Correspondence and requests for materials should be addressed to A.D.G. (agitler@stanford.edu).

Reviewer Information *Nature* thanks R. L. Juliano, J. Rothstein and T. Siddique for their contribution to the peer review of this work.

METHODS

Mouse crosses. *TDP-43* transgenic mice were generated by S. Kumar-Singh's laboratory and have been described previously[9,11]. *TDP-43*$^{Tg/+}$ mice were purchased from JAX (stock no.: 012836, B6;SJL-Tg(Thy1-TARDBP)4Singh/J). *TDP-43*$^{Tg/+}$ mice were maintained on a B6/SJL hybrid background by crossing with F1 hybrid mice from JAX to propagate the strain (stock no.: 100012, B6SJLF1/J). Ataxin-2 knockout mouse lines have been described previously[12,13]. *Atxn2*$^{+/-}$ mice created by G.A.'s laboratory were backcrossed to C57/BL6 mice for 10 generations and then maintained on the congenic C57/BL6 background by crossing with wild-type non-littermates within the same line. *Atxn2*$^{+/-}$ mice created by S.M.P.'s laboratory were maintained on a B6.129S hybrid background by crossing *Atxn2*$^{+/-}$ males with F1 hybrid females from JAX (stock no.: 101043, B6.129SF1/J). *Atxn2*$^{+/-}$ mice from G.A. or S.M.P. were crossed with *TDP-43*$^{Tg/+}$ mice in order to create lines A and B, respectively. Data for this project were collected from the offspring of *TDP-43*$^{Tg/+}$*Atxn2*$^{+/-}$, *TDP-43*$^{Tg/+}$*Atxn2*$^{+/+}$, and *TDP-43*$^{Tg/+}$*Atxn2*$^{-/-}$ mice each crossed with other non-littermate mice (to avoid genetic drift) of the same genotype, respectively, within the same line.

We collected data for lifespan, gait impairment, and other phenotypes in two independent trials for each line. These trials were performed 4 months apart with different breeding pairs. After we performed a search of current literature analysing lifespan in mouse models of neurodegenerative disease, we concluded that a total of 20 animals was probably a sufficient number in two separate trials to see an effect size worth additional consideration. The first trial of the study was performed with approximately ten animals per genotype. We intended to do a power analysis using data from this cohort, but the lifespan and the other behavioural analysis data were already statistically significant. Therefore, standard power analysis methods were no longer applicable. We repeated the study in a second trial for a final sample size of 18–28 animals (Fig. 1). All mice were genotyped through Transnetyx (Cordova, TN). Protein, RNA and histological analyses were performed using mice from line B. Approximately equal numbers of males and females were used in all analyses.

ASO validation and administration. We screened a collection of ASOs designed to target various regions of the mouse *Atxn2* mRNA[26]. After screening *Atxn2* ASOs for their ability to reduce *Atxn2* levels in cultured mouse cells, and for toxicity in wild-type mice, we tested several ASOs by delivering them through a single ICV injection into the brain of P1 mice[26], and used the most effective and well tolerated ASO for further studies. For the data presented in Fig. 4 and Extended Data Fig. 7d, i, P1 neonatal mice received an ICV injection of 3 μl of ASO in PBS (a total of 45 μg), mice were injected into the left ventricle using a NanoFil 10 μl syringe (World Precision Instruments) and a 33 gauge needle. The coordinates for injection were 2 mm anterior to the lambdoid suture, 1 mm lateral from the sagittal suture, and 2 mm deep. Within each litter, half of the pups (randomly chosen) were treated with a control ASO (CCTATAGGACTATCCAGGAA) and the other half were treated with an ASO that targeted mouse *Atxn2* (CTTCACATTTCGATCCAACA). Both ASOs were developed and synthesized by Ionis Pharmaceuticals. ASOs were synthesized as described[26] and were 20 bp in length, with five 2′-*O*-methoxyethyl modified nucleotides at each end of the oligonucleotide, and ten DNA nucleotides in the centre. The backbone of the ASOs consists of a mixture of phosphorothioate (PS) and phosphodiester (PO) linkages: 1-PS, 4-PO, 10-PS, 2-PO and 2-PS (5′ to 3′).

For the data presented in Extended Data Fig. 7a–c, e–h, wild-type mice were injected by ICV injection at P1 with 45 μg in 3 μl of *Atxn2* ASO or PBS control. Mice were euthanized at P28 for RNA analysis. Quantitative PCR for *Atxn2* mRNA was performed using the forward primer, CACTTCAGATTTCAACCCGAAC; reverse primer, TGACTGGTAGCGAGAAGGT; and probe TAGTTAATGG AGGTGTTCCCTGGCC. In an independent study to determine the safety of repeated injections of the *Atxn2* ASO, we injected wild-type mice at 5 weeks of age and again at 9 weeks then performed an observational study for 8 weeks. The animals moved normally within the cage, and did not have any overt tremor or gait impairment.

Care of the *TDP-43*$^{Tg/Tg}$ mice. Humane experimental protocols were performed as approved by the Administrative Panel of Laboratory Animal Care (APLAC) of Stanford University, an institution accredited by the Association for the Assessment and Accreditation of Laboratory Animal Care (AAALAC). In crosses where impaired *TDP-43*$^{Tg/Tg}$ mice were possible offspring, high-fat breeder chow was placed in the cage from P16–P21 to prepare the pups for prompt weaning. To avoid aggression towards the impaired *TDP-43*$^{Tg/Tg}$ mice by littermates and parents and to ensure the *TDP-43*$^{Tg/Tg}$ mice received adequate nutrition, all pups were weaned at P21. *TDP-43*$^{Tg/Tg}$ mice that had not reached the euthanasia end-point by this time were weaned into cages separate from other littermates. All *TDP-43*$^{Tg/Tg}$ mice were given wet food (Clear2O diet gel 76A) in a cup on the floor on of the cage from P21 until death to ensure that the impaired mice could easily chew their food and readily access food and water. Even severely impaired mice were observed eating, defecating and micturating. The mice were weighed every few days and no mice were found to weigh less than 75% of their maximum body weight.

Phenotype scoring and humane euthanasia end point determination. All phenotype scoring was performed blinded to the genotype or treatment group of the animal, and the order in which the animals were tested each day was random. Mice were placed on a textured plastic surface within an empty cage and observed as they moved around the cage. Gait impairment scoring was adapted from previously described methods[31]. The gait impairment score measures dysfunction, not overall motor proficiency, and is therefore translatable even to young mice. A score of 0, no impairment, was given if the mouse walked normally. A score of 1 was given if the mouse had a tremor or appeared to limp while walking. A score of 2 was given if the mouse had a severe tremor, severe limp, lowered pelvis, or feet pointing away from the body during locomotion (duck feet). A score of 3 was given if the mouse had difficulty moving forward, minimal joint movement, feet not being used to generate forward motion, difficulty staying upright, or its abdomen dragging on the ground.

A score of 4 marked the euthanasia end point in which the mouse fell over and was unable to right itself within 30 s on all 3 out of 3 trials. The end point was tested daily after a mouse had received a gait impairment score of 3. Some of the severely impaired mice took 10–15 min to be fully roused, and therefore, mice were not tested for the euthanasia end point until they were moving around their cage. A humane euthanasia end point was used instead of natural death in survival analysis for the welfare of the animals, but it also served as a more precise end point that is directly dependent on motor dysfunction (an ALS-relevant phenotype) and less dependent on insufficient food and water intake. The mice did not appear emaciated or severely dehydrated before euthanasia, nor did they dip below 75% of their maximum body weight. Body weight did not differ among *TDP-43*$^{Tg/Tg}$ *Atxn2*$^{+/+}$, *TDP-43*$^{Tg/Tg}$*Atxn2*$^{+/-}$, and *TDP-43*$^{Tg/Tg}$*Atxn2*$^{-/-}$ mice (Extended Data Fig. 1g). Seven of the sixty-six mice in the lifespan study were found dead before reaching the humane euthanasia end point. All of these mice were severely impaired (gait impairment score of 3) prior to death, and did not have any wounds that would suggest they were killed by cage mates. Two of the *TDP-43*$^{Tg/Tg}$*Atxn2*$^{-/-}$ mice in the lifespan study were euthanized at P84 for tissue collection. At the time of euthanasia, one had a gait impairment score of 0 and the other had a score of 3. As these two mice never reached the humane euthanasia end point, they are right-censored from the statistical analysis after the age of euthanasia as is appropriate for survival analysis. The age of death of these two mice is marked by upward ticks on Fig. 1b and Extended Data Fig. 1d. Three *TDP-43*$^{Tg/Tg}$*Atxn2*$^{-/-}$ mice were still alive at the time of paper submission. One was found dead at P472 after receiving a gait impairment score of 3. The other two were euthanized at P510 and P521 in order to conclude the study. Both had a gait impairment score of 1. One *TDP-43*$^{Tg/Tg}$ mouse injected with the *Atxn2* ASO at P1 was also alive at the time of paper submission and reached the humane euthanasia end point at P193. The ages of these four mice at the time of paper submission is marked by upward ticks on the graphs in Fig. 1d, Extended Data Fig. 1d, and Fig. 4d.

For the kyphosis score, if the mouse was able to easily straighten its spine as it walked, and did not have persistent kyphosis, it received a score of 0. If the mouse exhibited mild kyphosis, but was able to straighten its spine, it received a score of 1. If it was unable to straighten its spine completely and maintained persistent but mild kyphosis, it received a score of 2. If the mouse maintained pronounced kyphosis as it walked or while it sat, it was assigned a score of 3. Tremor was scored independently from 0 (not observed) to 3 (severe).

Mouse tissue collection. Anaesthetized mice were perfused with PBS and the brain and spinal cord were carefully dissected and washed in chilled PBS. The brain was cut in half sagittally. The brain hemisphere used for immunohistochemistry, as well as the cervical and lumbar enlargements of the spinal cord, were placed in 4% PFA in PBS at 4 °C for 48 h then stored in 30% sucrose in PBS for at least 24 h. The other brain hemisphere was cut into eight predefined sections. These brain sections and the remaining spinal cord segments (upper cervical, lower thoracic/upper lumbar and sacral) were flash-frozen in liquid nitrogen for later RNA or protein collection and stored at −80 °C. For all experiments using these samples (analysing RNA or protein), the investigator was blinded to the genotype of the animal during the protocol and the samples were processed in a random order. Only biological replicates from individual mice are plotted in graphs.

RNA extraction and qPCR. RNA was extracted using the PureLink RNA Mini Kit (Life Technologies user guide publication MAN0000406), using TRIzol reagent and on-column PureLink DNase I treatment. Surfaces and equipment were cleaned with RNaseZap and RNase-free pipette tips were used. In the first step of the protocol, flash-frozen tissue was kept on dry ice until 200 μl of TRIzol reagent was added. A Kontes motor pestle with a clean RNase-free disposable pestle was used to rapidly and thoroughly homogenize the sample (around 45 strokes). The rest of the TRIzol (800 μl) was then added and the sample was inverted to

mix. The remainder of the RNA isolation protocol was carried out as directed by the aforementioned user guide. The RNA was converted to cDNA using the High Capacity cDNA Reverse Transcription Kit. Standard TaqMan reagents, and the StepOnePlus Real-Time PCR System were used for qPCR with the following assays: human *TDP-43* (Hs00606522_m1), mouse *Atxn2* (Mm00485946_m1), and mouse *Actb* (Mm02619580_g1). Each reaction was performed in triplicate. The relative transcript levels were calculated in Excel by the following formula: (POWER (2, −(C_t mean target)))/(POWER(2, –(C_t mean *Actb*))).

Protein extraction. Nucleocytoplasmic fractioning was performed in a manner similar to that described previously[32]. All buffers were chilled and had Halt protease and phosphatase inhibitors, 1 mM DTT and 1 mM PMSF added right before use. Snap-frozen tissue was kept frozen on dry ice and precisely weighed. All subsequent volumes are based on this initial weight. From the addition of hypotonic buffer on, samples were kept chilled on ice. All centrifugation steps were performed in a 4 °C cold room. In brief, tissue was homogenized by around 30 strokes of a Kontes motor pestle in 200 µl hypotonic buffer (10 mM HEPES, 10 mM NaCl, 1 mM KH_2PO_4, 5 mM $NaHCO_3$, 5 mM EDTA, 1 mM $CaCl_2$, 0.5 mM $MgCl_2$). After homogenization, additional hypotonic buffer was added to a final volume of 10 µl mg^{-1}, and the tubes were inverted to mix. After 10 min on ice, 2.5 M sucrose (0.5 µl mg^{-1}) was added. The homogenate was pipetted up and down to resuspend and centrifuged at 6,300*g* for 10 min. The supernatant was collected as the cytoplasmic fraction. The pellet was washed four times in chilled TSE buffer (10 µl mg^{-1}; 10 mM Tris, 300 mM sucrose, 1 mM EDTA, 0.1% IGEPAL, pH 7.5). For each wash, the homogenate was pipetted up and down to resuspend, the tube was inverted to clean sides of tube, and the sample was centrifuged at 1,000*g* for 5 min. The supernatant was clear by the final wash. The pellet of nuclei was resuspended in chilled RIPA buffer (5 µl mg^{-1}; Sigma-Aldrich). The sample was homogenized by pipetting up and down and incubated on ice for 10 min. During this incubation, each sample was passed through a 21*G* needle 20 times to shear viscous chromatin in the solution. The samples were spun at 21,000*g* for 10 min, and the supernatant was saved as the nuclear fraction.

Sequential solubility fractioning was performed in a similar manner as described previously[33]. Extraction was performed on ice using chilled buffers until the urea buffer was added. Tissue was weighed. All subsequent volumes are based on this initial weight. RIPA buffer (5 µl mg^{-1}; Sigma-Aldrich) with Halt protease and phosphatase inhibitor and 5 mM EDTA added just before use, was added to the tissue chunk and thoroughly homogenized with a Kontes motor pestle for approximately 45 strokes. The homogenates were incubated on ice for 10 min and were transferred to polycarbonate centrifuge tubes. The samples were centrifuged (100,000*g*, 4 °C, 30 min) using a TLA 120.2 rotor. The supernatant was promptly and gently transferred to a new tube and stored at −80 °C. The pellet was washed by re-extraction in the same volume of RIPA buffer using the motor pestle for approximately 30 strokes. The samples were centrifuged again (100,000*g*, 4 °C, 30 min) and the supernatant was discarded. The pellets were extracted in urea buffer (2 µl mg^{-1}; 7 M urea, 2 M thiourea, 4% CHAPS, 30 mM Tris, pH 8.5) prepared just before the experiment, homogenized using a motor pestle for approximately 30 taps, and centrifuged (100,000*g*, 22 °C, 30 min). Supernatants were saved as the urea fraction and stored at −80 °C in aliquots.

Western blotting. Nuclear and cytoplasmic fractions were heated at 70 °C for 10 min with 1× LDS buffer. The protein concentration of the RIPA-insoluble fractions in urea buffer were measured using the Non-interfering protein assay kit (G Biosciences). Approximately 10 ug of each sample (1-5 µl) were mixed with 5 µl of 4× LDS loading buffer (Novex NuPage), and water to 20 µL total volume. The samples were not heated to avoid carbamylation. Proteins in LDS were run down 4–12% Bis–Tris gels and transferred to nitrocellulose membranes. The membranes were blocked in Odyssey blocking buffer (LI-COR) at room temperature for 1 h and treated over night at 4 °C with primary antibodies at the following dilutions: 1:5,000 rabbit TDP-43 C-terminal (Sigma-Aldrich T1580), 1:1,000 mouse human-specific TDP-43 (Novus Biologicals H00023435-M01), 1:1,000 goat lamin A/C (Santa Cruz 6215), 1:50,000 mouse GAPDH (Sigma-Aldrich G8795), 1:1,000 mouse ataxin-2 (BD 611378). Membranes were rinsed with PBST (0.1% Tween-20), washed three times for 10 min, and treated with 1:20,000 Alexa Fluor 680- or 790-conjugated IgG (H+L) raised in donkey (Life Technologies) at room temperature for 1 h, rinsed with PBST, and washed three times for 10 min before being developed on a LI-COR Odyssey scanner at laser intensity well below saturation.

Luminex assay. This assay was performed in the Human Immune Monitoring Center at Stanford University. Mouse 38-plex kits were purchased from eBiosciences/Affymetrix and used according to the manufacturer's recommendations with modifications as described below. In brief, beads were added to a 96-well plate and washed in a Biotek ELx405 washer. Samples were added to the plate containing the mixed antibody-linked beads and incubated at room temperature for 1 h followed by overnight incubation at 4 °C with shaking. Cold and room temperature incubation steps were performed on an orbital shaker at 500–600 r.p.m. Following the overnight incubation, plates were washed in a Biotek ELx405 washer and then a biotinylated detection antibody was added for 75 min at room temperature with shaking. The plate was washed as above and streptavidin-PE was added. After incubation for 30 min at room temperature, a wash was performed as above and reading buffer was added to the wells. Each sample was measured in duplicate. Plates were read using a Luminex 200 instrument with a lower bound of 50 beads per sample per cytokine. Custom-assay Control beads by Radix Biosolutions were added to all wells.

This assay was performed with brain tissue from P21 wild-type mice untreated ($n=5$) or treated at P1 by ICV injection with the *Atxn2* ASO ($n=4$) or control ASO ($n=5$). Each sample was processed in duplicate. The bead count and the coefficient of variation between duplicates were checked for each sample and epitope, and no cause was found to exclude values. Median fluorescence intensity (MFI) was averaged between the duplicates and normalized by dividing by the buffer background MFI for each respective epitope.

Mouse CNS histology. Fixed sections were mounted in OCT and cut to a thickness of 40 µm using a Leica CM3050 S Cryostat. Sections were stored in cryoprotective media (0.01 M sodium phosphate, 30% glycerin, 30% ethylene glycol) at −20 °C. Washes were done four times for 5 min each in TBST (0.1% Tween-20), unless otherwise noted, at room temperature. Washes and incubation steps were performed with gentle rotation using an orbital rotator. The following primary antibodies were used: 1:2,000 rabbit TDP-43 phospho 409/410 'pTDP-43 ab1' (Cosmo Bio, TIP-PTD-P01); 1:2,000 rabbit TDP-43 phospho 403/404 'pTDP-43 ab2' (Cosmo Bio, TIP-PTD-P05); 1:1,000 rabbit TDP-43 phospho 409/410 'pTDP-43 ab3' (a gift from L. Petrucelli's laboratory, affinity-purified 3655); 1:1,000 mouse TDP-43, human-specific (Novus Biologicals, H00023435-M01); 1:1,000 TDP-43 C-terminal (Sigma-Aldrich, T1580); 1:500 mouse NeuN (Millipore, MAB377); 1:1,000 rabbit NeuN antibody (abcam, ab177487); and 0.04 µg ml^{-1} rabbit TDP-43, mouse-specific (a gift from V. Lee's laboratory, 2341-aa379).

For DAB-amplified immunohistochemistry, free-floating sections were placed in a 12- or 24-well plate with a rectangular specimen net insert, washed, pretreated for 20 min at room temperature in TBST with 0.1% Triton X and 0.6% hydrogen peroxide, washed, and blocked in 10% normal goat serum for 1 h at room temperature. Primary antibody was diluted in TBST with 10% normal goat serum and incubated overnight at 4 °C. The sections were then washed, treated with biotinylated goat anti-rabbit IgG (H+L) secondary antibody (Vector) at 1:500 in TBST for 1 h at room temperature, washed, treated with an ABC kit (Vectastain) for 1 h at room temperature, and washed using 0.1 M Tris pH 7.4 for the final wash. DAB solution was prepared by dissolving a 10 mg DAB tablet (Sigma-Aldrich) in 20 ml of 0.1 M Tris pH 7.4. The solution was vortexed to dissolve, passed through a 0.45 µm filter unit, and 6 µl of 30% H_2O_2 was added right before use. All sections used in a single experiment were incubated simultaneously for 30 s to 2 min until the desired colour change was reached. Sections were washed four times with 0.1 M Tris for 5 min and mounted onto Superfrost Plus microscope slides (Fisher Scientific) in 0.1 M phosphate buffer pH 7.4 using a paintbrush. The slides were allowed to dry overnight and incubated in CitriSolv (Fisher Scientific) for a few minutes before immediate coverslipping with Entellan (Electron Microscopy Sciences). Sections were imaged using a Nikon Eclipse 50i microscope. pTDP-43 ab1 inclusions per section were quantified by hand at 20× magnification blinded to the identity of the mice. Mice were quantified in a random order, but for technical reasons, all spinal cord hemispheres for a single mouse were quantified at the same time. For each mouse, 14–26 lumbar spinal cord hemispheres were quantified with 6 mice per genotype.

Alternatively, the sections were stained for immunofluorescence microscopy. The sections were washed then blocked/pre-treated in TBST with 0.1% Triton X and 10% normal goat or donkey serum (depending on secondary antibody host) for 1 h at room temperature. Primary antibodies were diluted in TBST with 10% serum at 4 °C overnight. The sections were then washed, treated with Alexa Fluor-conjugated secondary antibodies (Life Technologies) diluted at 1:1,000 in TBST with 10% serum for 3 h, and washed again with Hoechst (1:5,000) added to the final wash. Sections were mounted on frosted slides in 0.1 M phosphate buffer pH 7.4 using a paintbrush, and when the sections were no longer visibly wet, the slides were coverslipped using Prolong diamond antifade mountant (Molecular Probes). Slides were stored at 4 °C for short term and −20 °C for long term.

High-quality representative images of inclusions identified using the pTDP-43 ab2 (Fig. 3f) were taken on a Zeiss LSM510 Meta Confocal microscope by generating a 10 µm *z* stack with 0.37-µm steps (maximal intensity projections are shown). Inclusions identified with pTDP-43 Ab2 were quantified using 44-µm-thick *z* stacks at 10× magnification (one spinal cord hemisphere per image) on a Leica DMI6000B fluorescent microscope. Maximum intensity projections were created using Fiji. Images were randomized and blinded by renaming each image

with a random number using python. Photoshop CS6 soft round brushes were used to occlude white matter and the dorsal horn. The images were then run through the MetaXpress granularity module to automatically quantify the number of inclusions per image in an unbiased manner. This method detects inclusions of a predetermined size range based on changes in surrounding pixel intensity. The optimal parameters for this experiment were empirically determined to be an approximate size range of 1.3–5.2 μm in diameter and pixel intensity change of 2,500 grey levels. The area of grey matter quantified in each image was measured using Fiji (the area quantified for each hemisphere was approximately 0.5 mm^2). The number of inclusions per image was divided by the area of that image, and these values were averaged for each mouse (average of 19 images per mouse).

To quantify diffuse nuclear TDP-43, spinal cord sections were stained with 1:1,000 TDP-43 C-terminal antibody, and imaged using a Leica DMI6000B fluorescent microscope. Using Fiji, a small circle was drawn in each nucleus (away from the inclusion, if an inclusion is present) to measure the diffuse TDP-43 signal. For *TDP-43*$^{Tg/Tg}$*Atxn2*$^{+/+}$ mice, cells with an obvious inclusion(s) and two nearby cells in the same focal plane without inclusions were quantified. For wild-type mice, five cells were quantified per image. There was no way to blind the experimenter, because the inclusions were either obviously present or absent in each image. Three mice per genotype were analysed, with an average of 18 images and 126 cells counted per mouse.

To quantify cortical layer V neurons, 40-μm-thick sagittal brain sections were processed for immunofluorescence, as detailed above, using a rabbit NeuN antibody. Images were taken at 5× using a Leica DMI6000B fluorescent microscope. Images were then blinded and processed in a random order. Quantification was performed using Fiji. Layer V was outlined using the polygon selection tool, 'measure' was used to find the area of the selection, a threshold was applied using the 'triangle' algorithm, the area outside the selection was removed using 'clear outside' and 'watershed' was used to separate overlapping nuclei. The 'analyze particles' tool was used to count nuclei that were greater than 50 μm in area and had a circularity from 0.2–1.0. The number of nuclei for each image was divided by the layer V area. For each mouse, 3–8 sections were quantified (see 'Statistical analyses').

Cell culture. To knockdown ataxin-2, Dharmacon ON-TARGETplus SMARTpool siRNA was used with the following target sequences: CCAAAGA GUAGUUAAUGGA, AAAGGUAUAUCACCAGUUG, GACAAGCCCUUC UUUCUAC, CUAAACGCAUGUCUUCAGA. Stress granule experiments were performed using 0.5 mM sodium arsenite in U2OS cells. Counting was done on a Leica Widefield microscope at 63×. Only cells with more than one EIF3η puncta and seemingly viable nuclei were considered. Cells with at least one TDP-43 puncta that co-localized with EIF3η were considered to be positive for TDP-43 granules, otherwise they were considered to be negative. Santa Cruz Biotechnology EIF3η (sc-16377) and Proteintech C-terminal TDP-43 antibody (12892-1-AP) were used for quantification. Phosphorylation-specific TDP-43 antibodies from Cosmo Bio (TIP-PTD-M01 and TIP-PTD-P05) and an ataxin-2 antibody (BD 611378) were also used for the stress granule images. TDP-43-positive stress granules were quantified at 60 min of sodium arsenite exposure. At this time point, almost all cells had stress granule formation, but the few without were excluded from quantification. 116–146 cells were counted per well for 3 separate wells for each siRNA used. The U2OS cell line was purchased from ATCC (HTB-96), an official cell line repository organization, and has not been validated since purchase. We tested the cell line for mycoplasma contamination by PCR in 2012, and it was negative. Since then, we regularly check for mycoplasma by DAPI staining, a method routinely used in the field. Mycoplasma-contaminated cells show DAPI-positive stain in the cytoplasm.

Statistical analyses. Analyses were performed using R version 3.1.3 and Prism 6 (GraphPad), and graphs were plotted using Prism 6. Survival curves were compared using the survdiff function in the survival R package, which performs a log-rank test, and effect sizes are reported as the hazard ratios given by the coxph function, which fits a Cox proportional hazards model. For comparisons among different genotypes or treatment groups, one-way ANOVA or two-tailed, unpaired *t*-tests were used when comparing three groups or two groups, respectively. For TDP-43 inclusion quantification, the number of inclusions per spinal cord section or image field was averaged for each animal. The animals were grouped by genotype and comparisons of interest were made between two groups using a two-tailed, unpaired *t*-test. All data analysed by ANOVA or *t*-test appeared to have a Gaussian distribution, and therefore parametric tests were used. If two groups compared by *t*-test appeared to have different standard deviations, an *F*-test was used to compare variances. We did not find any significant differences in variances among groups.

A two-way ANOVA was used to analyse Luminex 38-plex mouse cytokine assay data. Factor 1 was protein assayed; factor 2 was mouse treatment group. Pairwise comparisons among the three treatment groups were made for each protein. The Holm–Sidak method was used to compute multiplicity adjusted *P* values. All 114 pairwise tests were considered within one family.

Linear mixed models (LMM, implemented using the lme4 R package) were used to determine if genotype has an effect on cortical layer V neuron density or average neuron cell body area. The LMM helps alleviate the pitfalls of statistically comparing groups with small sample sizes, while appropriately taking into account that multiple measurements came from the same mouse. A likelihood ratio test was used to compare the null hypothesis including only random effects terms for mouse and anatomical section to the alternative hypothesis including these terms as well as a fixed effect for genotype. A similar LMM was used to determine whether the presence of an inclusion had an effect on the level of diffuse TDP-43 in neuronal nuclei. A likelihood ratio test was used to compare the null hypothesis including only random effects terms for mouse and image to the alternative hypothesis including these terms as well as whether an inclusion is present.

Whether mouse genetic background (line) affects lifespan was assessed using a Cox proportional hazards likelihood ratio test, comparing the null model including only genotype to an alternative model including genotype and line. The effect of sex on lifespan was tested analogously.

We assessed the evidence that supported the presence of two groups of responders (weak responders and strong responders) within the *TDP-43*$^{Tg/Tg}$*Atxn2*$^{-/-}$ population using two approaches, one Bayesian and one frequentist, both using the RStan R package. Both analyses suggest modest but significant support for two groups. In both analyses we compared how well a single Weibull distribution fit the *TDP-43*$^{Tg/Tg}$*Atxn2*$^{-/-}$ lifespan data compared to a mixture of two Weibull distributions. The Weibull distribution is a commonly used parametric survival model which generalizes the exponential distribution, with hazard function $\lambda p t^{p-1}$ where λ is the rate parameter, p is the shape parameter, and t is time.

In the Bayesian analysis, we estimated the Watanabe–Akaike information criterion (WAIC)[34] for the one- and two-component model using four chains of Hamiltonian Monte Carlo[35] with 2,000 iterations each, the first 1,000 of which were discarded as warmup. The difference in WAIC values was 3.3, suggesting positive support for the two-component model. In the frequentist analysis we consider the one- and two-component models as null and alternative hypotheses, respectively. We obtain maximum-likelihood estimates of the component parameters (shapes and rates) for the two models, using LBFGS and marginalizing over mixture assignments. We use the likelihood ratio between these two models as a test statistic. We used a parametric bootstrap, sampling 1,000 times from the empirical null (fit one component model) and refitting both models, to obtain the sampling distribution of the likelihood ratio. Under this distribution we obtain an empirical *P* value of 0.02 and thereby reject the one-component null hypothesis in favour of the alternative two-component hypothesis.

Data availability. The authors will make materials, data, code, and associated protocols promptly available to readers without undue qualifications. The ASOs used in this study are produced by IONIS pharmaceuticals, a for-profit company.

31. Guyenet, S. J. *et al.* A simple composite phenotype scoring system for evaluating mouse models of cerebellar ataxia. *J. Vis. Exp.* **39,** 1787 (2010).
32. Mitchell, J. C. *et al.* Wild type human TDP-43 potentiates ALS-linked mutant TDP-43 driven progressive motor and cortical neuron degeneration with pathological features of ALS. *Acta Neuropathol. Commun.* **3,** 36 (2015).
33. Walker, A. K. *et al.* Functional recovery in new mouse models of ALS/FTLD after clearance of pathological cytoplasmic TDP-43. *Acta Neuropathol.* **130,** 643–660 (2015).
34. Watanabe, S. Asymptotic equivalence of Bayes cross validation and widely applicable information criterion in singular learning theory. *J. Mach. Learn. Res.* **11,** 3571–3594 (2010).
35. Carpenter, B. *et al.* Stan: A probabilistic programming language. *J. Stat. Softw.* **76,** 1–32 (2017).

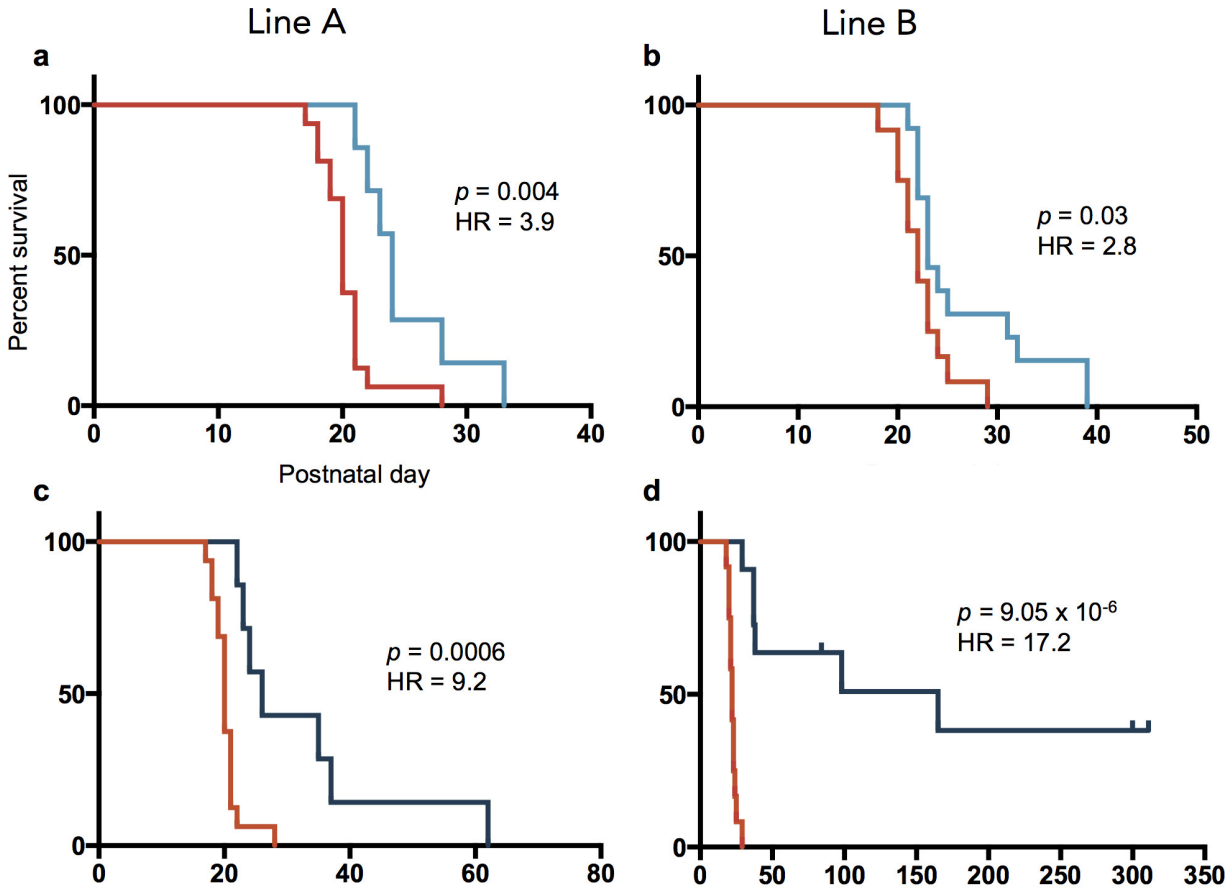

e

All *TDP-43*$^{Tg/Tg}$ mice

Lifespan models compared	Likelihood ratio test	Hazard ratio
Line + Genotype *vs* Genotype	p = .00065	Line A:B = 2.6
Sex + Genotype *vs* Genotype	p = .25	F:M = 1.4

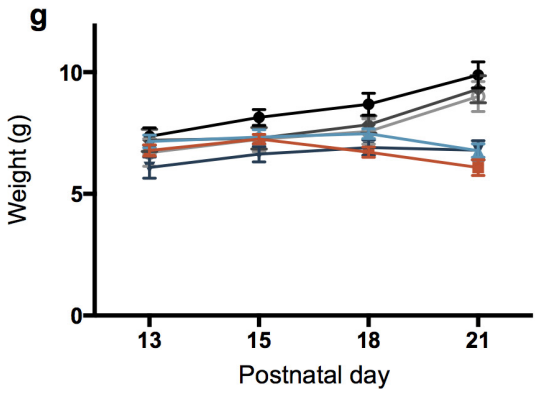

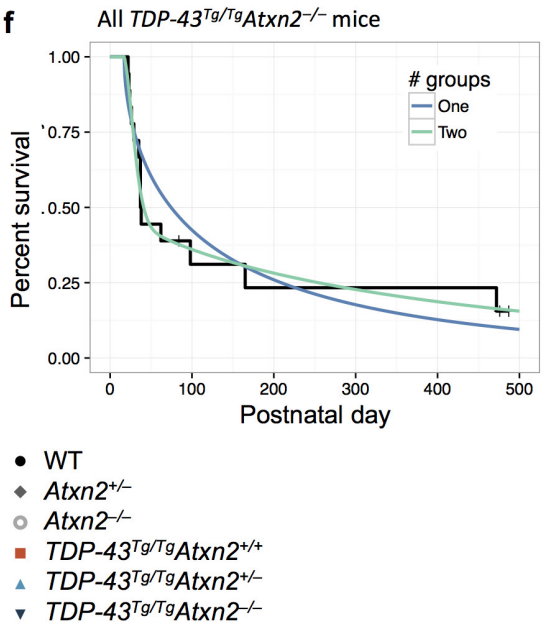

Extended Data Figure 1 | See next page for caption.

Extended Data Figure 1 | Reduction of ataxin-2 using two independent *Atxn2* knockout mice lines extends lifespan of *TDP-43* transgenic mice. **a**–**d**, Lines A and B were generated using $Atxn2^{+/-}$ mice from a congenic C57BL/6 and a hybrid B6.129S background, respectively. Within line A, $TDP\text{-}43^{Tg/Tg}Atxn2^{+/-}$ (light blue, $n = 7$) (**a**) and $TDP\text{-}43^{Tg/Tg}Atxn2^{-/-}$ (dark blue, $n = 7$) (**c**) mice lived significantly longer than $TDP\text{-}43^{Tg/Tg}Atxn2^{+/+}$ mice (red, $n = 16$). Within line B, $TDP\text{-}43^{Tg/Tg}Atxn2^{+/-}$ ($n = 13$) (**b**) and $TDP\text{-}43^{Tg/Tg}Atxn2^{-/-}$ ($n = 11$) (**d**) mice also lived significantly longer than $TDP\text{-}43^{Tg/Tg}Atxn2^{+/+}$ mice ($n = 12$). Curves were compared by log-rank test and effect size estimated by a Cox proportional hazards model. HR, hazard ratio. Ticks indicate mice that were euthanized for tissue collection before reaching the humane euthanasia end point or that were still alive at the time of submission (see Methods). **e**, After taking genotype into account, the line that the mice came from, but not the sex of the mice, significantly affected lifespan. A Cox proportional hazards likelihood ratio test was used to compare the null model including only genotype to an alternative model including genotype and line or genotype and sex. **f**, We found evidence for two groups of responders (strong and weak) in the $TDP\text{-}43^{Tg/Tg}Atxn2^{-/-}$ population (parametric bootstrap $P = 0.02$, see Methods). The Kaplan–Meier curve of all $TDP\text{-}43^{Tg/Tg}Atxn2^{-/-}$ mice from both lines is plotted, and the one and two group models are shown. **g**, Knockout of *Atxn2* did not affect weight in non-transgenic or $TDP\text{-}43^{Tg/Tg}$ adolescents. Data are mean ± s.e.m.

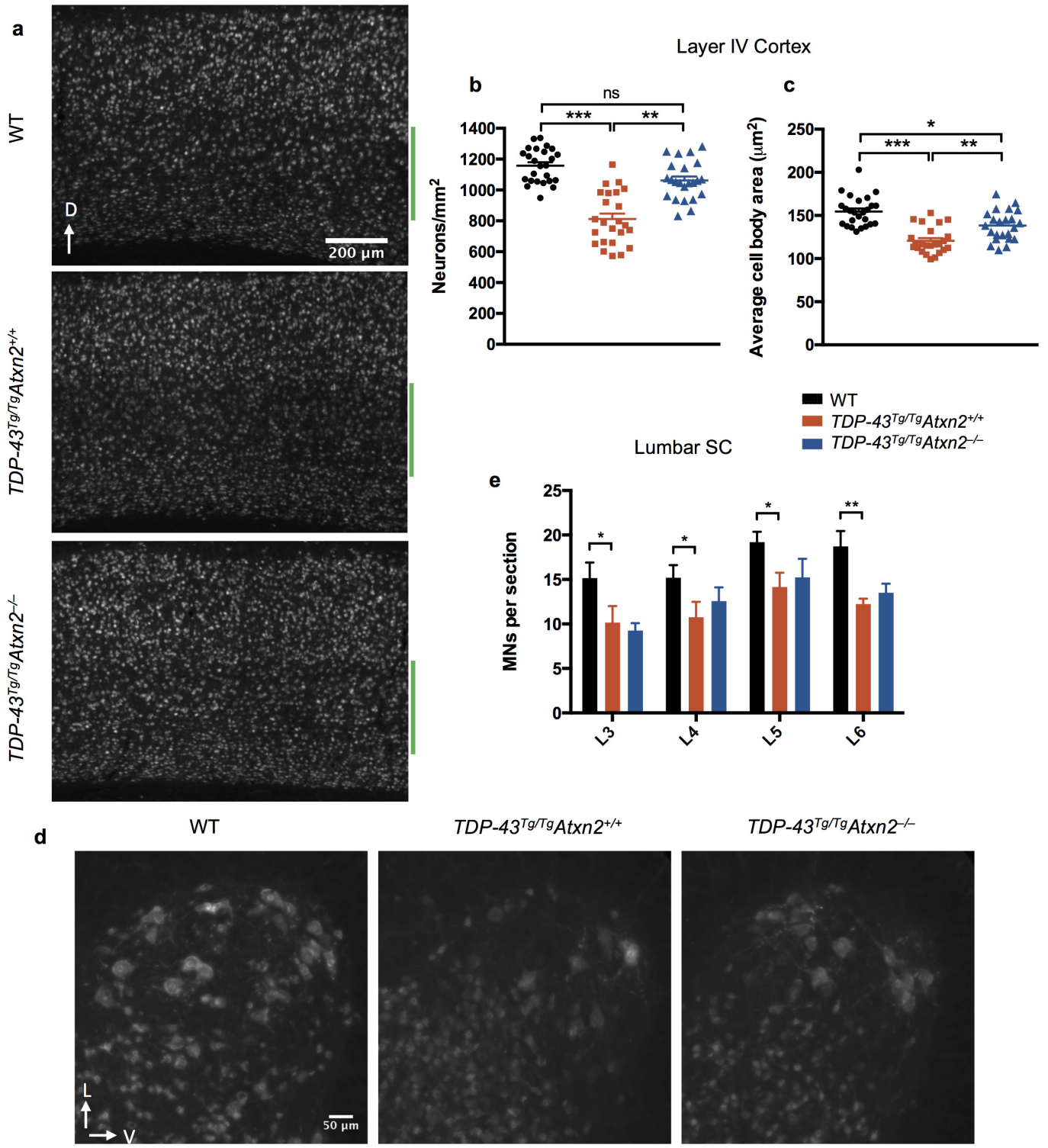

Extended Data Figure 2 | Cortical layer V and lower motor neuron loss in *TDP-43* transgenic mice. a, Representative NeuN stains of a sagittal section through the cortex. Layer V is marked by a green bar. **b**, **c**, Layer V neurons were 30% less numerous (**b**) and had smaller cell bodies (**c**) in *TDP-43*$^{Tg/Tg}$*Atxn2*$^{+/+}$ mice. These phenotypes were significantly ameliorated in *TDP-43*$^{Tg/Tg}$*Atxn2*$^{-/-}$ mice. Four mice were quantified per genotype, and the values for individual brain sections are plotted. Genotype groups were compared using linear mixed models with a random effect to appropriately account for the multiple measurements per mouse (see Methods). **d**, Representative NeuN stains of L5 lumbar ventral horn showing large lower motor neurons. **e**, Quantification of motor neuron cell bodies present in the ventral horn of the lumbar enlargement at levels L3–L6. There was a 27% decrease in motor neurons on average in *TDP-43*$^{Tg/Tg}$*Atxn2*$^{+/+}$ compared to wild-type mice. Six P23 animals were used per genotype. Two-tailed *t*-tests were performed between groups of interest. Data are mean ± s.e.m. $^{*}P < 0.05$; $^{**}P < 0.01$; $^{***}P < 0.001$; NS, not significant.

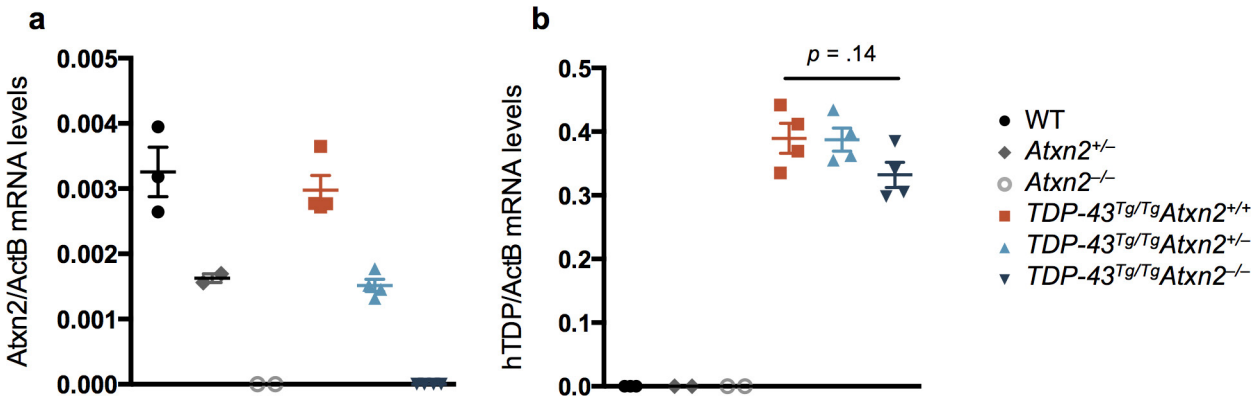

Extended Data Figure 3 | Lowering ataxin-2 levels does not affect expression of the human *TDP-43* transgene. a, *Atxn2* mRNA levels were decreased in the $Atxn2^{+/-}$ mouse brain by approximately 50% and completely absent in $Atxn2^{-/-}$ mice. **b**, Among $TDP\text{-}43^{Tg/Tg}$ mice, *Atxn2* reduction did not significantly affect levels of the human *TDP-43* (hTDP) transgene by ordinary one-way ANOVA. Samples were collected at P21. Data are mean ± s.e.m.

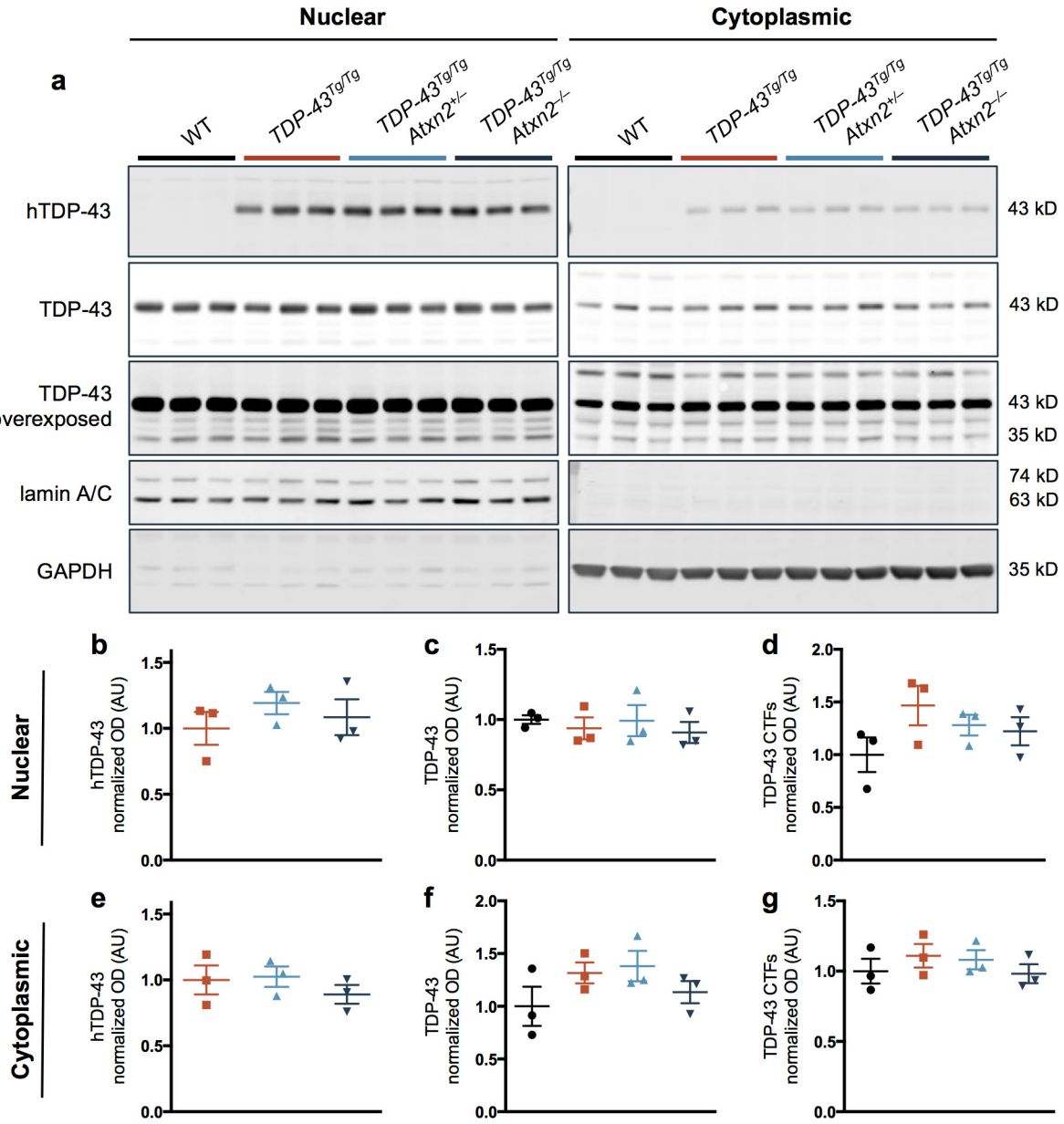

Extended Data Figure 4 | Protein levels of TDP-43 are not significantly affected by ataxin-2 reduction in *TDP-43$^{Tg/Tg}$* mice. **a**, Nucleocytoplasmic fractioning of mouse brain tissue segregated the nuclear marker lamin A/C from the cytoplasmic marker GAPDH. **b–d**, Nuclear levels of human TDP-43 (hTDP-43; **b**) or total full-length TDP-43 (**c**) were not altered among the genotypes, although nuclear TDP-43 CTFs were slightly elevated in *TDP-43$^{Tg/Tg}$Atxn2$^{+/+}$* mice (**d**). **e–g**, Cytoplasmic hTDP-43 (**e**) and total TDP-43 CTFs (**g**) were also unaltered among the genotypes, although cytoplasmic full-length TDP-43 (**f**) seemed slightly elevated in *TDP-43$^{Tg/Tg}$Atxn2$^{+/+}$* mice. Samples were collected at P21. Data are mean ± s.e.m. Gel source data can be found in Supplementary Fig. 1.

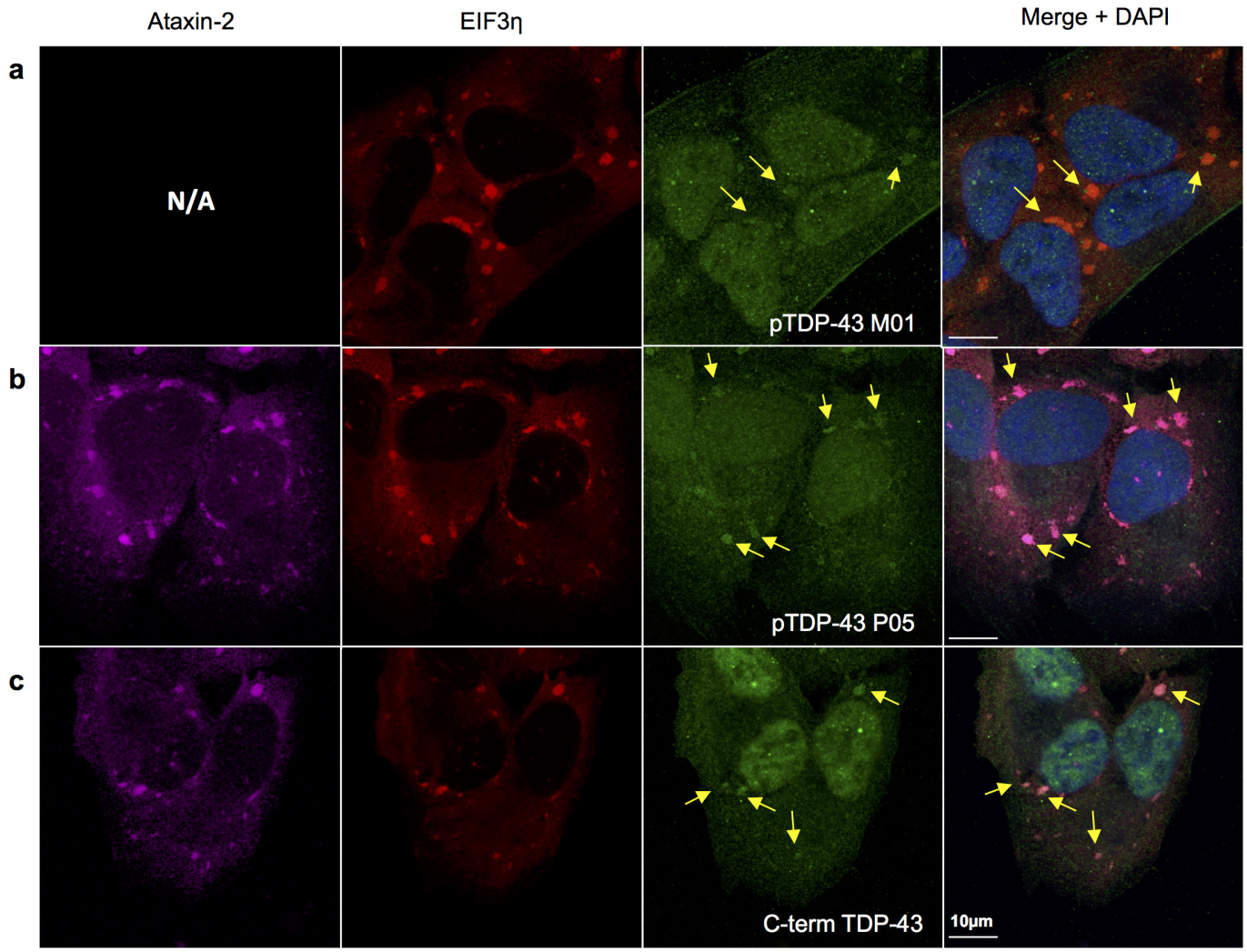

Extended Data Figure 5 | Stress granules contain phosphorylated TDP-43. a–c, Two different phosphorylation-specific TDP-43 antibodies (**a, b**) and a C-terminal epitope TDP-43 antibody (**c**) readily stained stress granules, indicated by the stress granule markers EIF3η and ataxin-2.

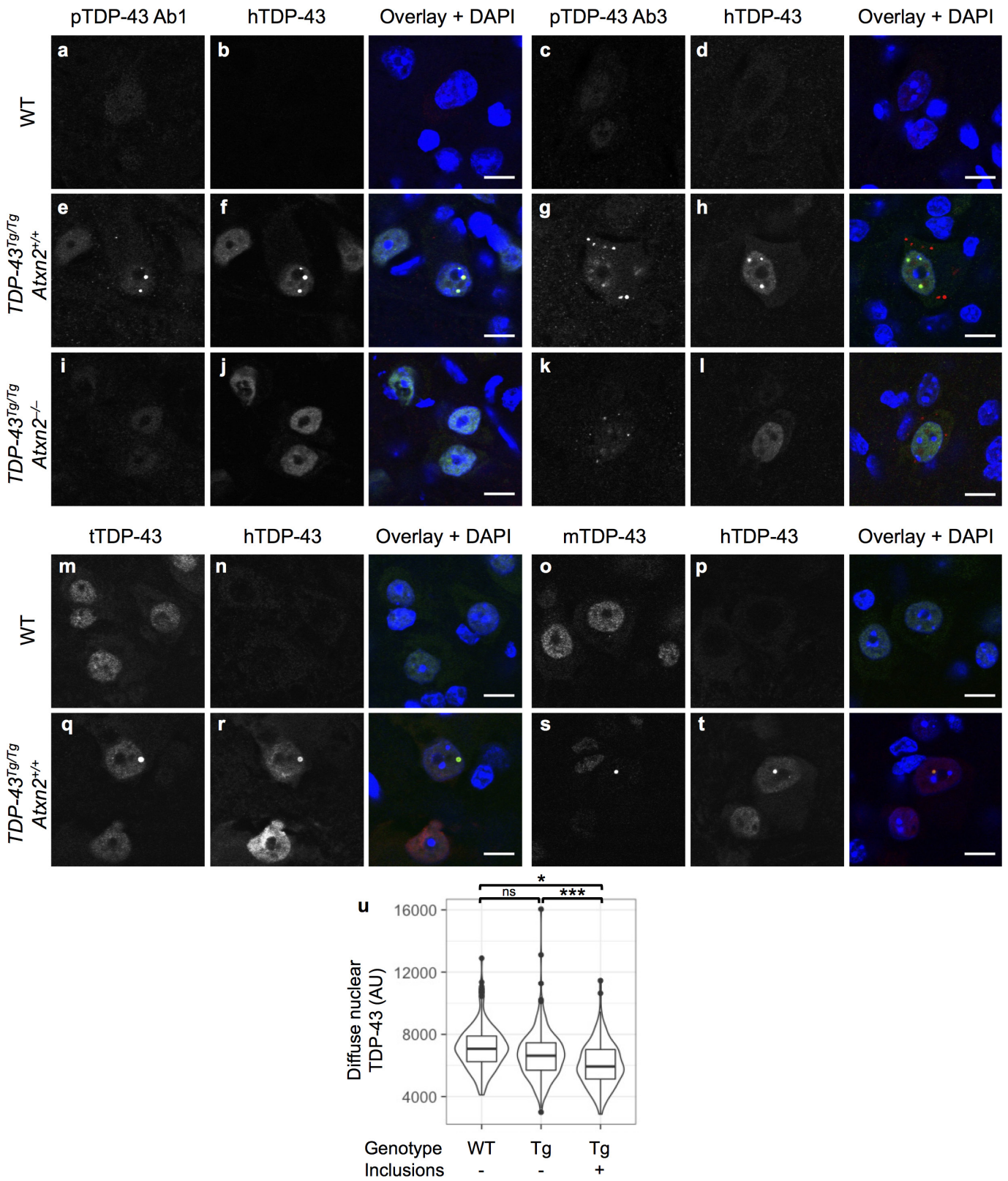

Extended Data Figure 6 | See next page for caption.

Extended Data Figure 6 | Two different types of inclusions are recognized in *TDP-43$^{Tg/Tg}$* mice. a–d, m–p, None of the TDP-43 antibodies tested recognized inclusions in wild-type mice. **e**, **f**, **h**, **q–t**, One of the three phosphorylated TDP-43 (pTDP-43)-specific antibodies (**e**) and TDP-43 antibodies that were not phosphorylation-specific (**f**, **h**, **q–t**) recognized spherical, predominantly nuclear inclusions. **g**, The other two pTDP-43-specific antibodies (only one is shown) recognized smaller cytoplasmic and nuclear inclusions (**g**). **i**, **j**, **l**, The first type of inclusion was very rare in *TDP-43$^{Tg/Tg}$Atxn2$^{-/-}$* mice. **k**, The second type of inclusion appeared smaller and reduced in number in *TDP-43$^{Tg/Tg}$Atxn2$^{-/-}$* mice. **q–t**, Nuclear inclusions were effectively stained with total TDP-43 (tTDP-43), human-specific TDP-43 (hTDP-43), and mouse-specific TDP-43 (mTDP-43) antibodies. **s**, Diffuse mTDP-43 is greatly decreased in *TDP-43$^{Tg/Tg}$* mice, an expected outcome of TDP-43 autoregulation. **u**, Levels of diffuse nuclear tTDP-43 were quantified by immunofluorescence microscopy in wild-type neurons or TDP-43$^{Tg/Tg}$ neurons with or without inclusions. These three groups were compared in a pairwise fashion using linear mixed models with a term to appropriately account for multiple measurements per mouse ($n = 3$ mice per genotype, see Methods). Median and minimum to maximum are plotted. Images were taken of cervical spinal cord. Samples were collected at P21. Scale bars, 10 μm.

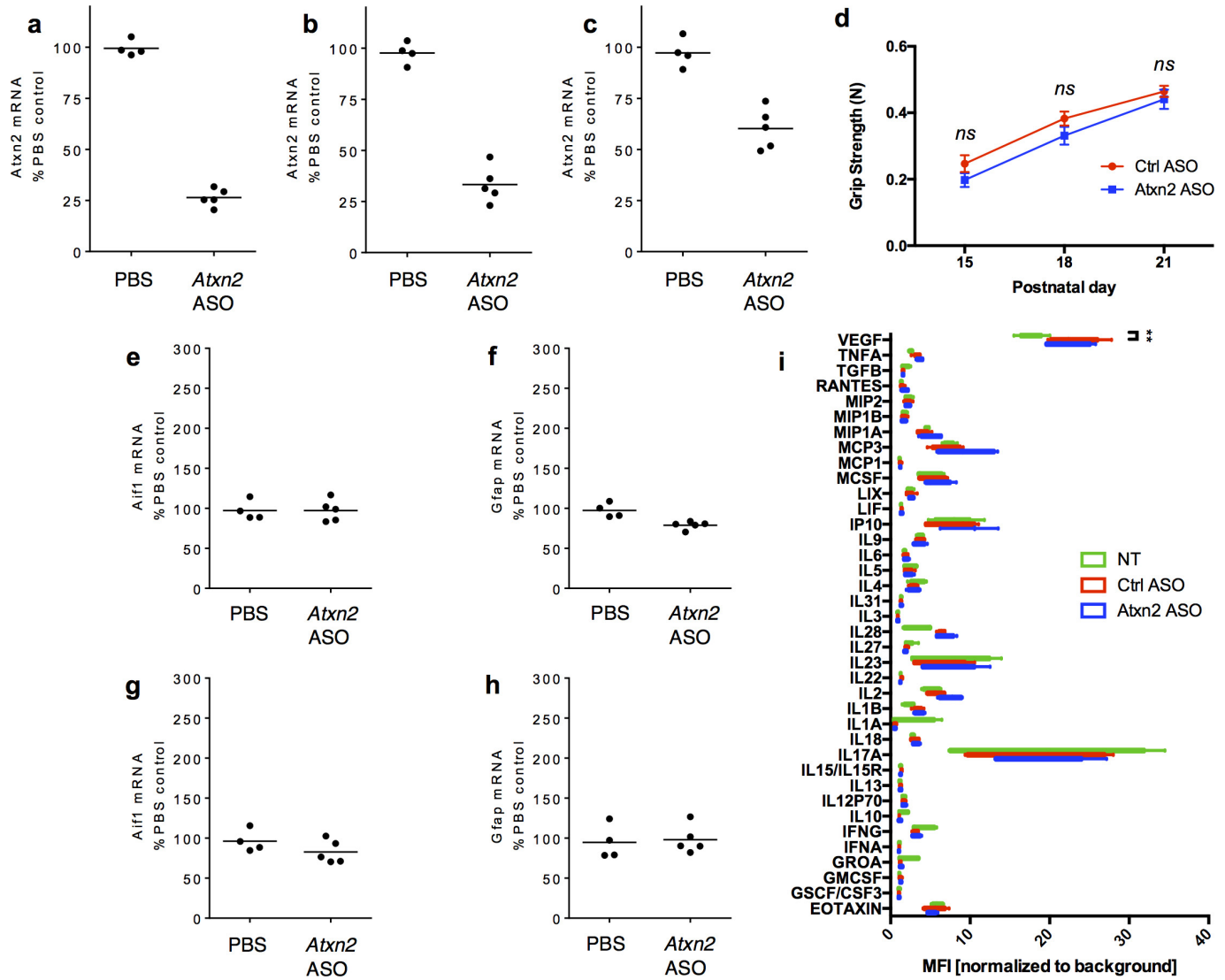

Extended Data Figure 7 | An ASO that targets *Atxn2* is able to successfully reduce mRNA levels throughout the central nervous system. a, ICV injection at P1 of an ASO that targets *Atxn2* was able to successfully reduce levels of *Atxn2* mRNA in the spinal cord by approximately 75% when assessed at P28. **b**, **c**, *Atxn2* reduction was also seen in the cortex (**b**) and cerebellum (**c**). **d**, Grip strength of wild-type mice was not effected by injection of control (Ctrl) or *Atxn2* ASOs ($n = 16$ mice per treatment). Data are mean ± s.e.m. **e**–**h**, Genetic markers of gliosis, *Aif1* and *Gfap*, were not altered in the spinal cord (**e**, **f**) or cortex (**g**, **h**) after ASO injection. **a**–**c**, **e**–**h**, Biological replicates and mean are shown. **i**, Using a Luminex 38-plex assay, we could not detect a significant difference in inflammatory markers among uninjected wild-type mice ($n = 5$) and wild-type mice treated with the *Atxn2* ($n = 4$) or control ($n = 5$) ASOs (two-way ANOVA treatment group factor $P = 0.32$). However, the ASO-treated animals had a small increase in 1 of the 38 markers, VEGF. Multiplicity-adjusted pairwise tests revealed that this difference was not significant for mice treated with the *Atxn2* ASO ($P = 0.17$), but was for mice treated with control ASO ($P = 0.006$). Minimum to maximum are shown.